Article

Not peer-reviewed version

In vitro and Reactive Metabolites Investigation of Metabolic Profiling of Tyrosine Kinase Inhibitors Dubermatinib in HLMs by LC–MS/MS

Nasser Salem Al-Shakliah *, Rashad Alsalahi, Hatem Abuelizz, Adnan A. Kadi

Posted Date: 15 May 2023

doi: 10.20944/preprints202305.1022.v1

Keywords: N-methyl piperazine; Dubermatinib; In vitro metabolites; Cyano adducts; GSH conjugate; Xenosite reactivity model

Article

In Vitro and Reactive Metabolites Investigation of Metabolic Profiling of Tyrosine Kinase Inhibitors Dubermatinib in HLMs by LC–MS/MS

Nasser S. Al-Shakliah *, Adnan A. Kadi, Hatem A. Abuelizz and Rashad Al-Salahi

Department of Pharmaceutical Chemistry, College of Pharmacy, King Saud University, P.O. Box 2457 Riyadh, 11451, Saudi Arabia; nassersalem30@yahoo.com

Abstract: Dubermatinib (DMB, TP-0903), a benzenesulfonamide, is an inhibitor of the tyrosine kinase AXL, which is a member of the TAM family, and can prevent GAS6-mediated activation of AXL in cancer cells. Patients with previously treated chronic lymphocytic leukemia are being studied in phase I/II clinical trials to determine its antineoplastic potential (CLL). In the current work, the reactive intermediates of DMB were studied using liquid chromatography-mass spectrometry (LC-MS). Human liver microsomes (HLMs) were exposed to dimethylbenzene in a laboratory setting, and the resulting metabolites were collected through protein precipitation. Intense reactivity toward nucleophilic macromolecules was seen in the metabolites of the piperazine and pyrimidine rings in DMB, iminium and 2,5-quinone-imine, respectively. To assess the toxicities of the possibly reactive metabolites, DMB was incubated with HLMs in the presence of 1.0 mM KCN and 1.0 mM glutathione. The DMB metabolites found by LC-MS/MS were seven in vitro phase I metabolites, three cyano adducts, and two GSH conjugates. Phase I in vitro metabolic reactions included N-demethylation, hydroxylation, and dechlorination. The in vitro metabolism of DMB and the metabolites it produces have not been studied before.

Keywords: N-methyl piperazine; Dubermatinib; In vitro metabolites; Cyano adducts; GSH conjugate; Xenosite reactivity model

1. Introduction

Drugs belonging to the tyrosine kinase inhibitor (TKI) class selectively inhibit kinase activity by modifying intracellular signals required for the growth of cancer cells1. As regulatory enzymes, tyrosine kinases (TKs) switch various cellular processes on and off by transferring gamma phosphate groups from ATP to the hydroxyl groups of target proteins2. Phosphorylation of proteins by kinases is a crucial signal for controlling cellular activities like cell division and the phosphorylation of proteins often occurs at serine or threonine residues. Dubermatinib (DMB, TP-0903) inhibits tumor cell proliferation and migration by blocking AXL-mediated signal transduction pathways and so inhibiting epithelial-mesenchymal transition (EMT). Reductions in tumor cell proliferation and migration accompany inhibition of the TAM family of receptor tyrosine kinases (TYRO3, AXL, and MERTK), which play critical roles in tumor cell proliferation, survival, invasion, and metastasis3. DMB is being studied in a phase I/II clinical trial in patients with previously treated chronic lymphocytic leukemia (CLL) and has been shown to inhibit tumor cell motility, survival, invasion, proliferation, colony formation, and chemotherapeutic sensitivity4,5. A phospho-kinase array of DMB-treated cells demonstrated an increase of greater than 50% in p53 S392 and Chk-2 T68 phosphorylation, as well as a similar increase in histone H2AX phosphorylation in a model of neuroblastoma6. Patients with advanced metastatic or progressive solid tumors and acute lymphocytic leukemia (AML) are currently participating in phase I/II trials to evaluate the dosage, safety, pharmacodynamics, and pharmacokinetics of DMB (Clinical Trial Identification Numbers: NCT02729298, NCT04518345, and NCT03013998).

Liquid chromatography-mass spectrometry (LC-MS) was performed to differentiate and describe in vitro DMB metabolites. Moreover, the generated reactive metabolite(s) can covalently

Preprints (www.preprints.org) | NOT PEER-REVIEWED | Posted: 15 May 2023 doi:10.20944/preprints202305.1022.v1

alter proteins, which is regarded the initial step in producing drug-induced organ toxicities. This study was conducted to determine whether or not reactive metabolites could aid in the prediction of the toxicities of DMB and its pharmacological relatives. Mass spectrometry fails to detect reactive metabolites in vivo due to their ability to bind to endogenous components including DNA and proteins7. Our team has previously investigated the production of reactive metabolites by TKIs. This work was expanded upon in the current investigation, which demonstrated that DMB generated five reactive intermediates via two distinct bioactivation pathways. The reactive metabolites created were isolated, identified, and the bioactivation pathways were determined using two distinct trapping agents. As shown in Figure 1, the N-methyl piperazine ring is a defining structural feature of DMB. Compounds containing this moiety were shown to be metabolically bioactivated to yield the iminium intermediates that are attacked by potassium cyanide as a nucleophile to afford the cyano adducts8. The halogenated benzene ring in DMB undergoes metabolic bioactivation via oxidation, resulting in the reactive intermediate 2,5-quinone-imine, which can be addressed by glutathione 9. The objective of this study was to extract, identify, and isolate these stable adducts and conjugates of DMB using LC-MS10–12. These reactive metabolites helped us to estimate the toxicity of DMB13. The molecular basis of DMB in vitro biotransformation and changes in the properties of the metabolites relative to the parent compound were investigated by performing in silico drug metabolism. When compared to experimental stages for metabolic and toxicity profiles, in silico methods are less expensive and take less time to complete14–16. The Xenosite CYP450 model was used to anticipate susceptible metabolic sites in the DMB chemical structure (Figure 1), as well as to detect the bioactive center and structural alarms in the DMB structure, both of which improved its safety and efficacy in a variety of targets.

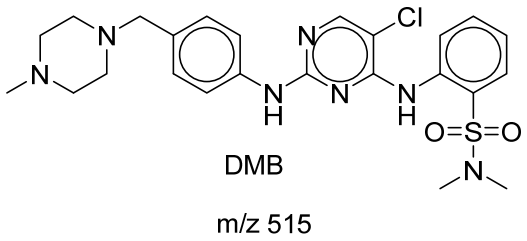

Figure 1. Chemical structure of DMB

2. Materials and Methods

2.1. Chemicals

Milli-Q was connected to the Elix Millipore water purification system to obtain water (Millipore, USA). BDH laboratory supplies was the source for magnesium chloride (MgCl2) and sodium hydroxide (NaOH) (Poole-UK). ACROS produced Nicotinamide adenine dinucleotide phosphate (NADPH). WINLAB, UK supplied potassium dihydrogen phosphate (KH2PO4) and sodium dihydrogen phosphate (NaH2PO4). Sigma-Aldrich supplied glutathione reductase (GSH), acetonitrile (ACN) HPLC-grade, formic acid (HCOOH), and potassium cyanide (KCN) (USA). The dubermatinib (TP-0903) was acquired from Med Chem (Princeton, NJ, USA). Male liver microsomes (M0567) were obtained from the company Sigma-Aldrich (West Chester, PA, USA). The HLMs were kept at 70 °C until their use. HLMs contained 20 mg/mL of protein in a solution of 250 mM sucrose. HepaRGTM Cryopreserved Cells (HPRGC10) were purchased from ThermoFisher (Waltham, MA USA).

2.2. Chromatographic conditions

The separation was accomplished using an Agilent 1290 series system comprised of a G1311A quaternary pump, a G1322A degasser, a G1367B HIP-ALS autosampler, a G1316A thermostatted column compartment, and an agilent 6495C mass spectrum. We employed a mobile phase of 0.1% formic acid in water (A) at a pH of 4.5 and 0.1% formic acid in acetonitrile solvent (B) in conjunction

 doi:10.20944/preprints202305.1022.v1

with an eclipse plus C18 (2.1 150 mm 3.5 m) column. The water/acetonitrile mixture was subjected to gradient chromatography for 85 minutes at a flow rate of 0.2 mL/min. When the program began, 95% of solvent A was employed, and then within 60 minutes, the percentage of solvent B was increased from 5% to 60% and then remained constant for the following 20 minutes. A 5 L sample was fed into the HPLC apparatus. Drying gas was nitrogen, gas temperature was 350 degrees Celsius, gas flow was 11.0 liters per minute, nebulizer pressure was 55 pounds per square inch, ESI was used as the ion source, capillary voltage was 4,000 volts, and the mode was positive in the MS.

2.3. Xenosite web predictor for in silico prediction

Available and free online software is utilized to estimate the likely metabolic locations of xenobiotics and other tiny chemical compounds. It suggests that nine key CYP450 isoenzymes, including 1A2, 2B6, 2A6, 2C9, 2C8, 2D6, 2C19, and 3A4, as well as human liver microsomes, are involved (HLM). The software has a quick runtime, and the metabolism produced site score correlates closely with potential metabolite [17,18]. For the metabolism produced site prediction, the DMB chemical structure in SMILES format was uploaded to the website.

In silico studies were performed using the XenoSite reactivity model, which can be downloaded for free from http://swami.wustl.edu/xenosite, to identify sites where reactive intermediate[17] might potentially cause damage. More than 680 molecules were used in neural networks to create this predicted model. The software's speedy execution time is one of its many advantages[19].

2.4. In vitro metabolism of DMB

Twenty HLMs from human livers were treated with DMB in a manner similar to that previously described[20]. The HLMs were prepared by adding a 0.08 M phosphate buffer to a stock solution of dimethyl benzene in dimethyl sulfoxide (DMSO) (pH 7.4). To begin, the components were shaken together in a water bath preheated to 37 degrees Celsius for 5 minutes to ensure that they were well-mixed. The incubation procedure was initiated with a solution of nicotinamide adenine dinucleotide phosphate (NADPH). In a final incubation mixture volume of 1 mL, the drug concentration was 30 M, the NADPH concentration was 1 mM, and the microsomal protein concentration was 1 mg/mL. NAPDH was substituted with a buffer solution, and the microsomal protein was used as a positive control. After 90 minutes of incubation, 2 mL of ice-cold acetonitrile was added to end the reaction and precipitate the proteins. Next, the samples were centrifuged at 21,900 g for 10 minutes. Re-containerization and evaporation of the supernatant in a stream of nitrogen. After reconstituting the residue in mobile phase, it was sent to vial HPLC for analysis. In order to catch reactive intermediate metabolites, the identical procedure was carried out with either 1.0 mM glutathione (GSH) or 1.0 mM KCN. To ensure reliability, the same methods were applied to testing negative controls as to testing positive ones. The activity of the microsomal preparation was measured against a concentration of phenytoin (2 M).

3. Results and Discussion

3.1. DMB metabolism and reactivity (in silico prediction)

DMB SOMs suggested the most essential isoenzymes of CYP450, which include 1A2, 2A6, 2B6, 2C8, 2C9, 2C19, 2D6, 2E1, 3A4, and HLM. The outcomes of DMB's in silico SOM predictions are displayed in Figure 2. The results were presented graphically, with details such as the strength of the color gradient and the bar representing the color scale. The greatest possible SOM score for a given atomic site is 1, hence a red color suggests a high probability of metabolism at that site, whereas a white color indicates no metabolism at that location. Two methyl groups of sulphonamide, N-methyl-piperazine, and carbons linked to the nitrogens of piperazine have been identified as possible atomic sites for metabolism in the DMB structure. These results agreed with experimental work that measured seven in vitro phase I metabolites (M1-M7), as well as cyano adducts and GSH conjugates.

Preprints (www.preprints.org) | NOT PEER-REVIEWED | Posted: 15 May 2023 doi:10.20944/preprints202305.1022.v1

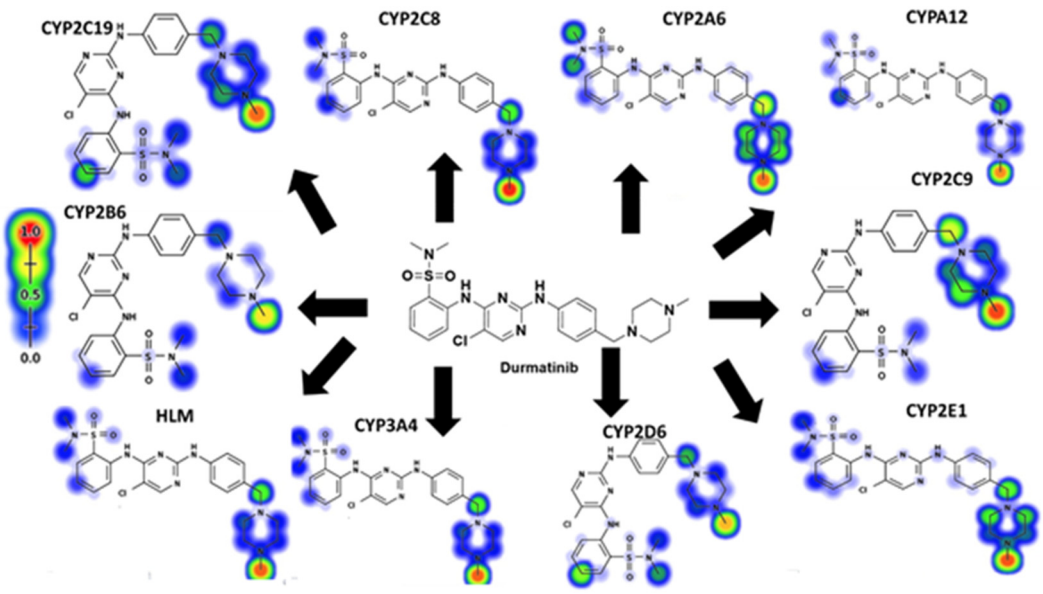

Figure 2. Predicted atomic sites of metabolism for DM B by Xenosite web predicto.

Figure 3 displays the results of the Xenosite web page's cyano and GSH model's prediction of DMB reactivity. This effort was directed by a list of proposed metabolites and reactive intermediates that was generated using in silico hypotheses and previous knowledge from the literature. The cyano reactivity model predicts the most probability of N-methyl-piperazine and the carbons connected to piperazine nitrogens, while the GSH reactivity model predicts the highest chance of 5-chloropyrimidine bioactivation. The theoretical reactivity results agree with experimental observations. As the color's intensity suggests, other potential bioactivation sites are not particularly high on the list of priorities.

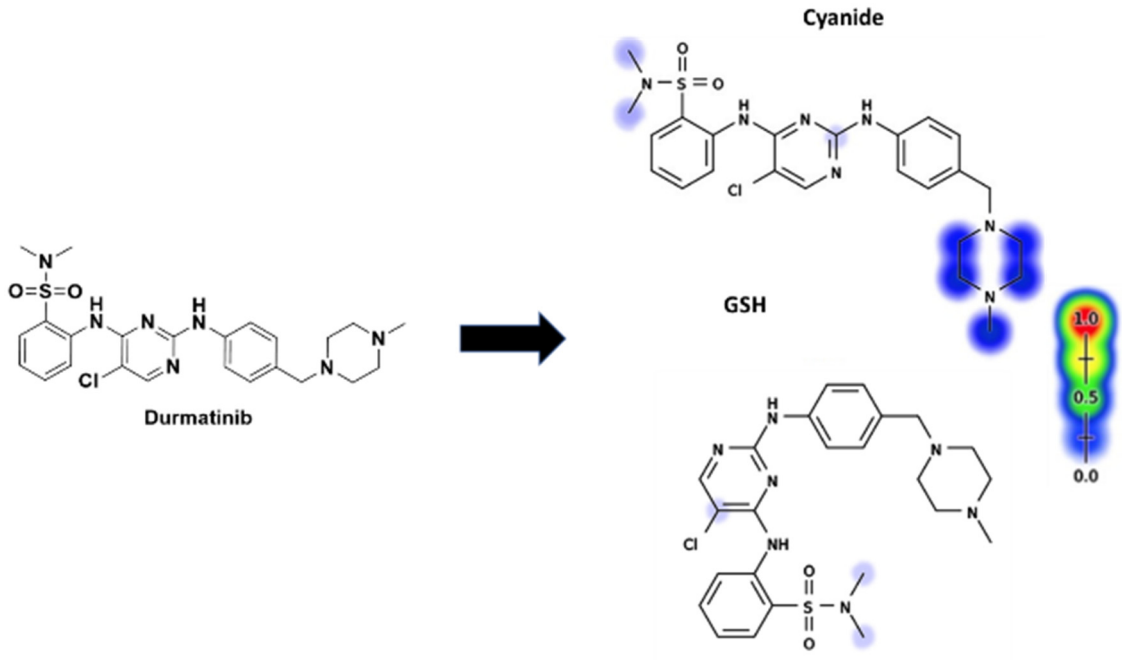

Figure 3. Predicted bioactive sites of DMB by Xenosite web predictor including GSH and cyano bioactive centers.

3.2. DMB fragmentation

Parent ion peak (PIP) of DMB appeared at 29.5 minutes in total ion chromatogram (TIC). PI fragmentation at m/z 516 yielded two daughter ions at m/z 313 and 206 (Figure 4A). The molecular

Preprints (www.preprints.org) | NOT PEER-REVIEWED | Posted: 15 May 2023 doi:10.20944/preprints202305.1022.v1

structure of DMB was divided into two parts, labeled A (in red) and B (in blue), to assist in the identification of specific metabolic reactions (Figure 4B).

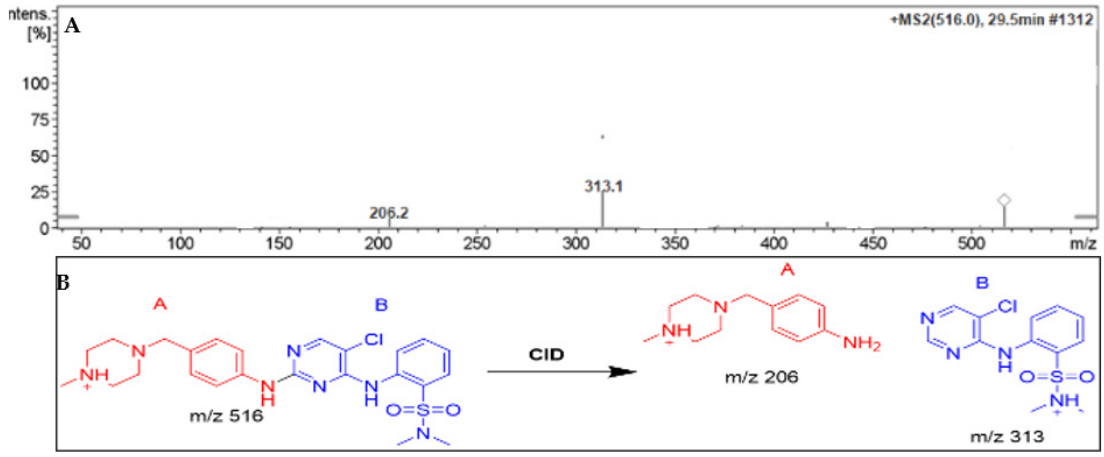

Figure 4. Positive ion MS/MS of DMB at 29.5 min. (A). Fragment ions of DMB (B).

3.3. Phase I metabolites of DMB identified in vitro

Seven different phase I metabolites were found:

- M1 and M2 (N-demethylation metabolites) at (m/z: 502)
- M3 (m/z = 474) was found to be the only metabolite with triple N-demethylation.
- M4 (m/z = 532) was shown to be a hydroxylated metabolite.
- M5 at (m/z 498), a product of dechlorination and hydroxylation, has been isolated.
- The metabolite M6 at (m/z: 484) has been shown to undergo N-demethylation, dechlorination, and hydroxylation.

One metabolite, designated M7 at (m/z: 514), was shown to be the product of dechlorination and double hydroxylation (Table 1). Figures S1–S6 (supplementary file) are provided for M2, M3, M4, M5, and M7. These three metabolic reactions occurred after DMB was incubated with HLMs, resulting in the seven metabolites: N-Deethylation, N-Dichloromethylation, and O-Hydroxylation[21].

Table 1. Phase I metabolites of DMB identified in MS and MS/MS scans.

	MS scan	**Major daughter ions**	**tR (min)**	**Proposed metabolic reaction**
DMB	516	206, 313	29.5	DMB+H
M1	502	313,192	22.7	N-demethylation at piperazine ring
M2	502	299,206	23.1	N-demethylation at sulphonamide group
M3	474	192,285	24.4	N-demethylation at piperazine ring and sulphonamide group
M4	532	313,222,117	25.1	α hydroxylation at piperazine ring
M5	498	295,206,98	27.5	dechlorination then hydroxylation
M6	484	295.192	28.1	dechlorination then hydroxylation and N-demethylation at piperazine ring

Preprints (www.preprints.org) | NOT PEER-REVIEWED | Posted: 15 May 2023 doi:10.20944/preprints202305.1022.v1

M7	514	295,222,117	28.6	dechlorination followed by hydroxylation at pyrimidine and hydroxylation at piperazine ring

3.3.1. The DMB M1 metabolites identification

At 22.7 min, we have seen the M1 PIP, which indicated DMB N-demethylation. Collision-induced dissociation (CID) fragmented the molecular ion peak (MIP) at m/z 502, yielding ions at m/z 313 and 192. (Figure 5A). Similarly to the other fragment ions at m/z 313, the m/z 192 daughter ion suggests that the N-demethylation occurred at the DMB piperazine ring (Figure 5B).

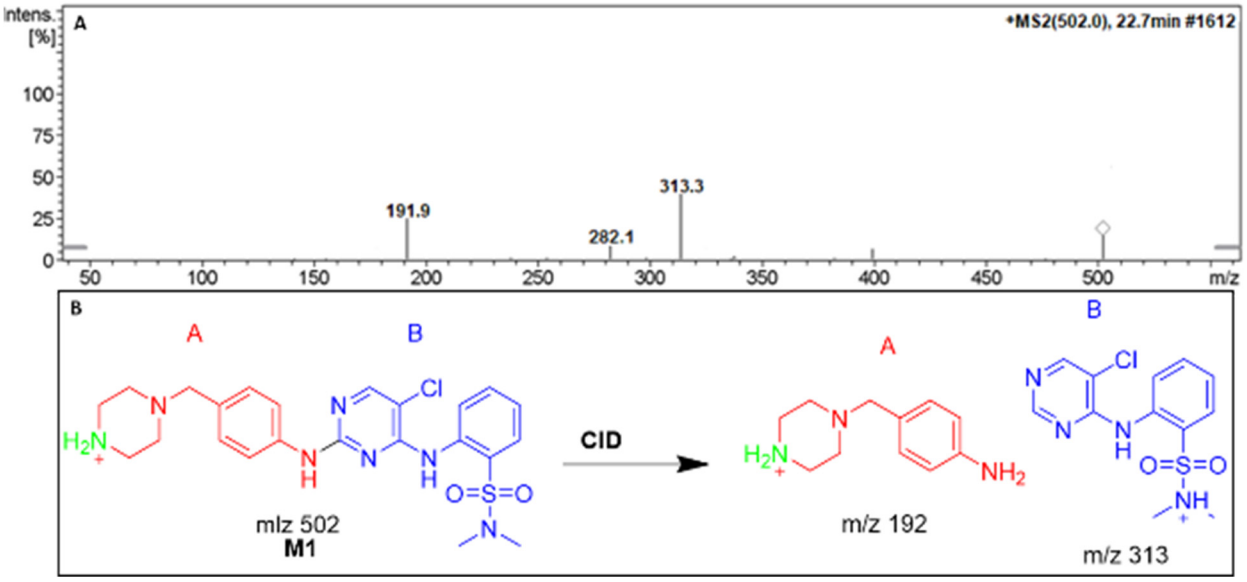

Figure 5. Positive ion MS/MS of M1 at 22.7 min. (A). Fragment ions of M1 (B).

3.4. Identification of in vitro DMB reactive metabolites

The identical metabolic interaction between DMB and HLMs was carried out to capture iminium and 2,5 quinone-imine intermediates in the presence of 1.0 mM KCN and 1.0 mM GSH, respectively. Bioactivation and subsequent trapping by cyano and GSH nucleophiles of the N-methyl piperazine and pyrimidine rings of the DMB structure are illustrated in Table 2 [22, 9] . The mass spectral information for all DMB reactive metabolites has been saved as a separate file (Figure S7-S11).

Table 2. DMB Reactive metabolites.

	MS scan	**Most abundant fragment ions**	**Rt (min)**	**Metabolic reaction**
Cyano adducts				
DMB541CN	541	126, 231, 313,514	35.2	Attack of KCN at bioactivated N-methyl piperazine ring
DMB527CN	527	217, 313,500	37.0	N-demethylation and attack of KCN at bioactivated N-methyl piperazine ring.
DMB513CN	513	126, 231, 285	38.1	Double N-demethylation at sulphonamide group and attack of KCN at bioactivated N-methyl piperazine ring.
GSH conjugates				

Preprints (www.preprints.org) | NOT PEER-REVIEWED | Posted: 15 May 2023 doi:10.20944/preprints202305.1022.v1

DMB803GSH	803	206, 496,600	41.5	Conjugation of GSH at bioactivated 2,5quinone-imine
DMB789GSH	789	206,308,586	42.6	N-demethylation at sulphonamide and conjugation of GSH at bioactivated 2,5quinone-imine

3.4.1. Identification of the DMB541CN cyano adduct reactive metabolite of DMB

After 35.2 minutes, the DMB541CN PIP was detected. Cyano nucleophiles may have attacked the bioactivated piperazine ring in DMB541CN during the metabolic reaction that occurred there. Daughter ions at m/z 126, 231, and 313 were produced by the DMB541CN CID at m/z 541 (Figure S7). Loss of hydrogen cyanide molecules (27 Da) was compatible with the cyano addition, as suggested by the PI at m/z 541. The cyanide adduct was confirmed, and the elimination of the HCN was suggested, by a neutral loss at mass m/z 27 (Figure S7). The cyanide ion was added to the N-methyl piperazine ring, as evidenced by the resulting ions at m/z 126, 231, and 313 (Scheme 1).

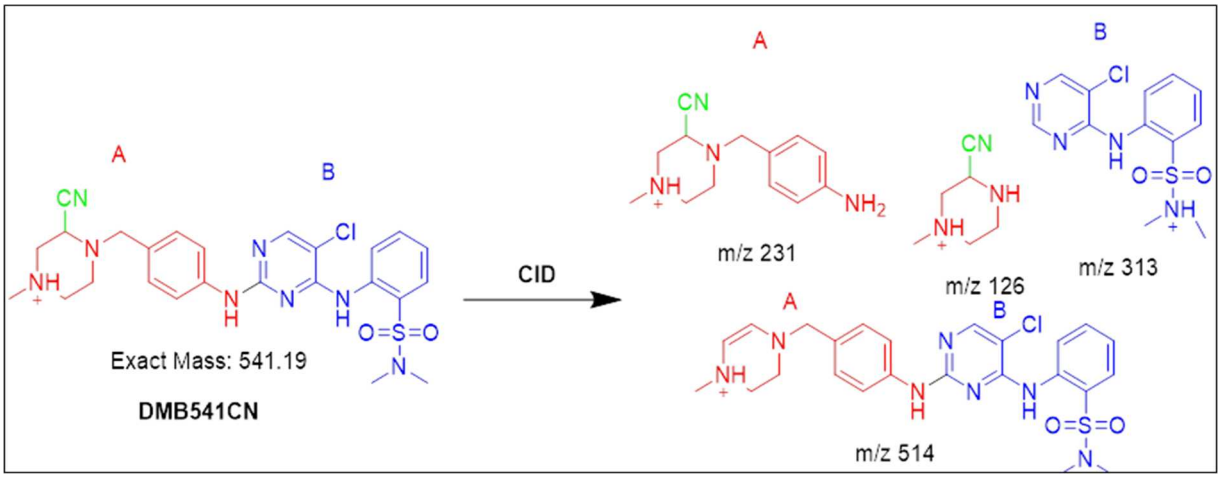

Scheme 1. Fragmentation pattern of DMB541CN [M+H]- at m/z = 541.

3.4.2. Identification of the DMB527CN cyano adduct reactive metabolite of DMB

At 27 minutes, a PIP for the DMB527CN was displayed. N-demethylation and the attack of cyano nucleophiles on the bioactivated piperazine ring occurred as metabolic reactions in DMB527CN, leading to the formation of the cyano adduct. Three distinctive product ions with mass numbers of 500, 313, and 217 were generated when the DMB527CN CID ion was excited at mass number 527 (Figure S8A). Indicated by PI at m/z 500, the loss of hydrogen cyanide molecules (27 Da) was consistent with the cyano addition. The cyanide adduct was confirmed, and the elimination of the HCN was suggested, by a neutral loss at mass m/z 27 (Figure S8B). The m/z 313 and 217 ion peaks, when compared to PIs of DMB, showed that the N-methyl piperazine ring had been modified by the addition of cyanide (Scheme 2)

Preprints (www.preprints.org) | NOT PEER-REVIEWED | Posted: 15 May 2023 doi:10.20944/preprints202305.1022.v1

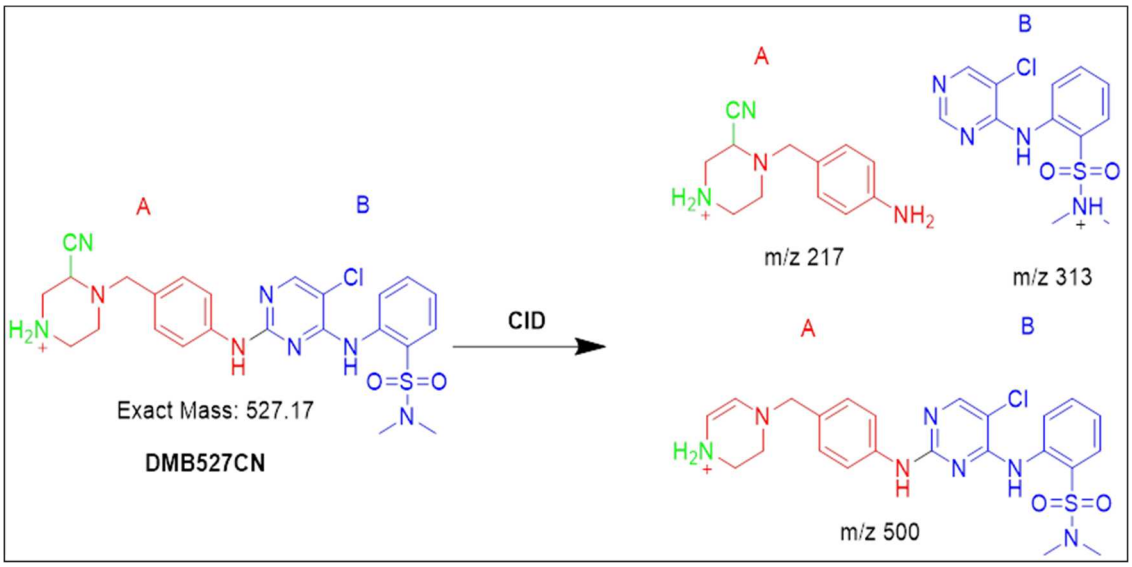

Scheme 2. Fragmentation pattern of DMB527CN [M+H]- at m/z = 527.

3.4.3. Identification of the DMB513CN cyano adduct reactive metabolite of DMB

At 38.1 minutes, the DMB513CN showed up. The metabolic reactions that occurred in DMB513CN suggested that the cyano adduct was afforded by N-demethylation at the sulphonamide group and the attacking of cyano nucleophiles on the bioactivated piperazine ring. At m/z 513, four distinct product ions 486, 213, 126, and 285, were generated through collision-induced dissociation (CID) of the parent DMB513CN ion (Figure S9A). PI at m/z 486 indicates the disappearance of hydrogen cyanide molecules (27 Da). The cyanide adduct was confirmed, and the elimination of the HCN was suggested, by a neutral loss at mass m/z 27 (Figure S9B). The addition of cyanide ion at the N-methyl piperazine ring was confirmed by the product ions at m/z 126, 213, and 285, which were compared to PIs of DMB (Scheme 3).

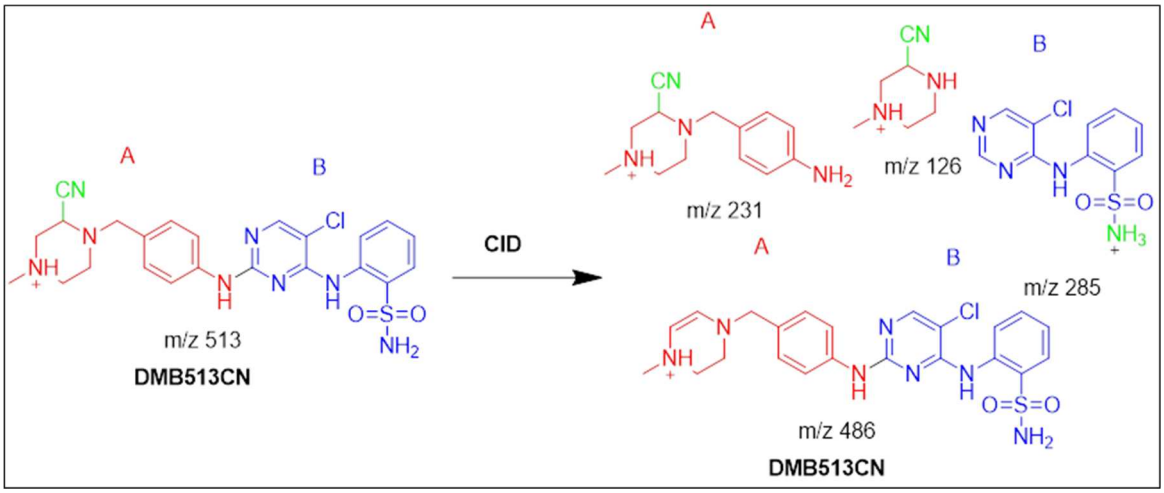

Scheme 3. Fragmentation pattern of DMB513CN [M+H]- at m/z = 513.

3.5. Identification of DMB GSH conjugates

3.5.1. Identification of the DMB803GSH conjugate DMB

Around 41.5 minutes in, the DMB803GSH was appeared. DMB803GSH's metabolic pathways pointed to dechlorination, hydroxylation, and conjugation of GSH at 2,5- quinone-imine (Scheme4). The production of DMB803GSH from DMB in vitro suggested the formation of 2,5-quinone-imine. DMB803GSH, a CID ion at m/z 803, decomposed into m/z 600, 496, and 206 ions

Preprints (www.preprints.org) | NOT PEER-REVIEWED | Posted: 15 May 2023 doi:10.20944/preprints202305.1022.v1

(Figure S10A). The synthesis of conjugated GSH was confirmed by the presence of a molecule ion at m/z 496. In relation to DMB PIs, the resultant ions at m/z 600 and 206 validated the conjugation GSH at the DMB pyrimidine ring (Scheme4). Another LC-MS/MS screening for the GSH conjugate was done by constant neutral loss scan monitoring of ions that lost 307 Da 22 (Figure S10B) [23] .

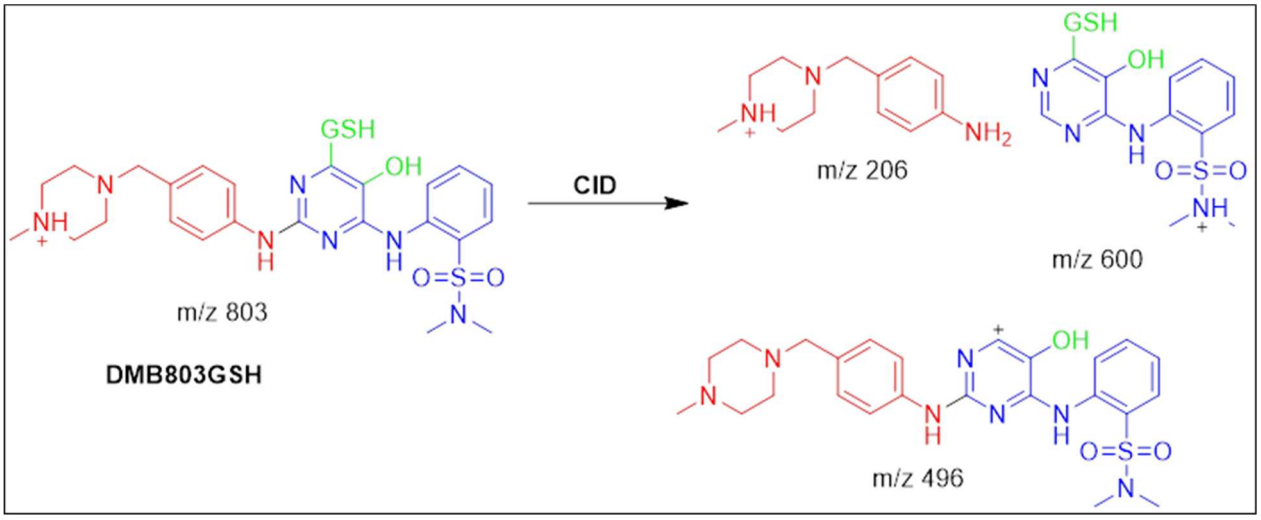

Scheme 4. Fragmentation pattern of DMB803GSH [M+H]- at m/z = 803.

3.5.2. Identification of the DMB789GSH conjugate DMB

At 42.6 minutes, the DMB789GSH was started to appear. The metabolic pathways that were active in DMB789GSH were anticipated to be N-demethylation at the sulphonamide group, dechlorination, hydroxylation, and GSH conjugation at the 2,5-quinone-imine (Scheme 5). In vitro DMB metabolism, as evidenced by the production of DMB789GSH, resulted in the synthesis of 2,5-quinone-imine. The m/z 789 DMB789GSH CID ion decomposed into four m/z 660, 586, 308, and 206 fragment ions (Figure S11A). Pyroglutamic acid cleavage yields an ion at m/z 660 (129 Da) that agrees with a GSH conjugation being generated (Scheme 5). The m/z 586 and m/z 206 ionic fragments of the same molecule revealed GSH conjugation at the DMB pyrimidine ring and hence their relationship to PIs of DMB (Figure S11B). The m/z 308 resultant ion represents the dissociation of GSH conjugation (Figure S11B). Constant neutral loss scan monitoring of ions that lost 307 Da was used in another round of LC-MS/MS screening for the GSH conjugate (Figure S11B) [22].

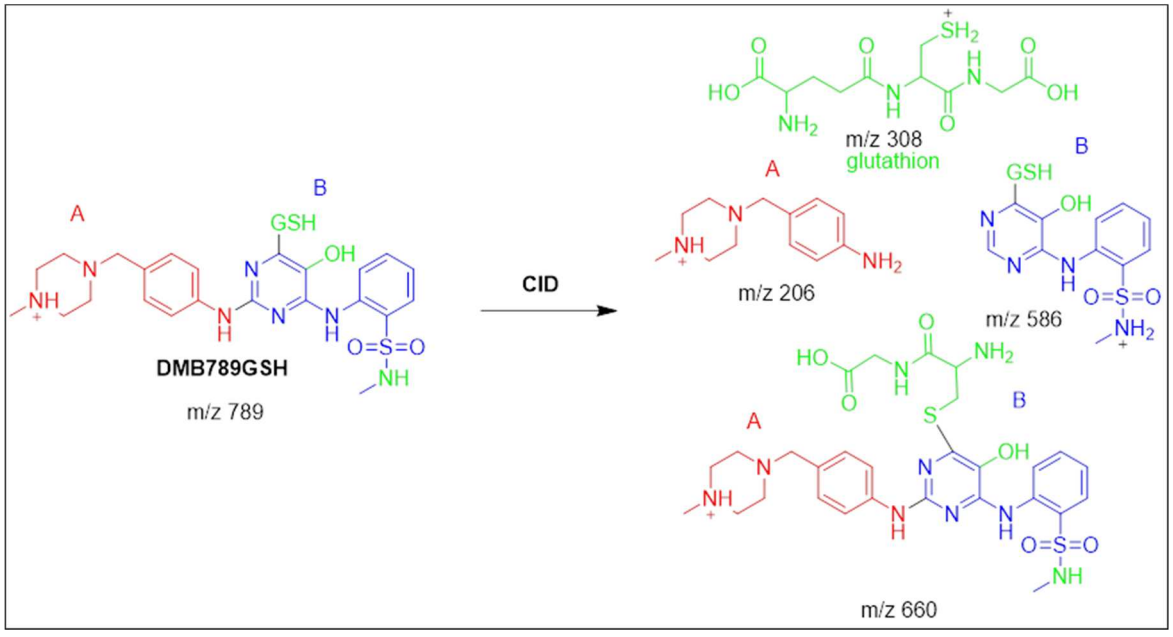

Preprints (www.preprints.org) | NOT PEER-REVIEWED | Posted: 15 May 2023 doi:10.20944/preprints202305.1022.v1

Scheme 5. Fragmentation pattern of DMB789GSH [M+H]- at m/z = 789.

3.6. Proposed bioactivation pathways of DMB

Figure 6 depicts possible bioactivation pathways for DMB. Cyanide adducts (DMB541CN, DMB527CN, and DMB513) detected in DMB during metabolism suggested that iminium intermediates were formed at the N-methyl piperazine ring. It was hypothesized that the bioactivation mechanism involved hydroxylation at DMB N-methyl piperazine, followed by dehydration, to produce the iminium ion intermediate as a highly reactive and unstable nucleophile. To isolate these reactive intermediates, KCN was used, and LC-IMS was then used to identify the stable cyanide adducts that resulted. The bioactive mechanism of the iminium intermediate [9, 14, 21] has been studied using cyclic tertiary amine-containing drugs. In order to validate the formation of 2,5-quinone-imine intermediates in DMB metabolism, glutathione (GSH) was used as a trapping agent. We anticipated that GSH producing conjugates like DMB803GSH and DMB789GSH [24,9] may target the bioactivation process comprising dechlorination, hydroxylation, and oxidation to produce 2,5-quinone-imine (Figure 6).

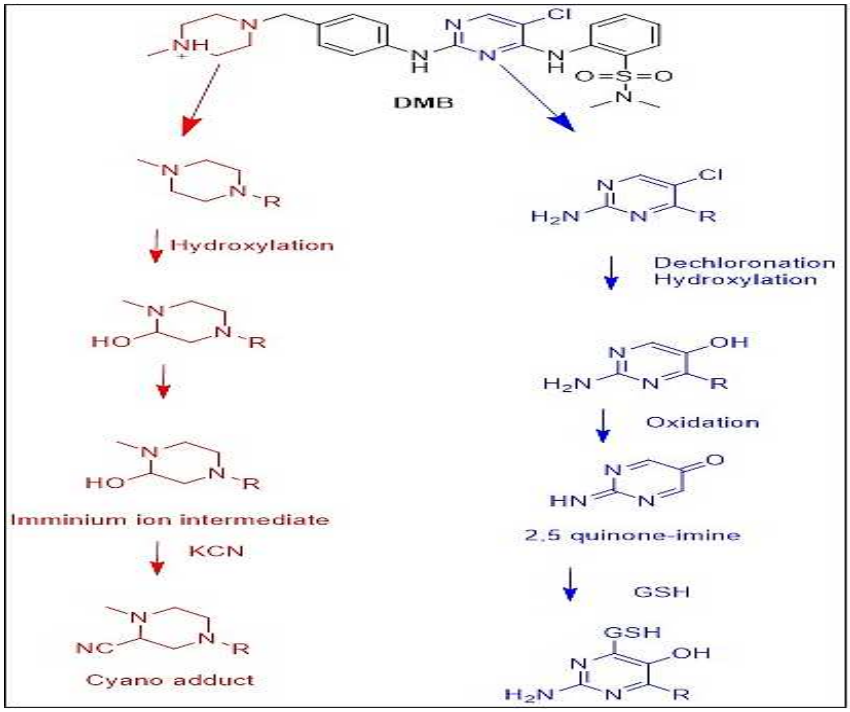

Figure 6. Proposed pathways for DMB bioactivation.

4. Conclusions

Seven phase I metabolites of DMB have been identified in vitro. Phase I metabolic reactions were found to include N-demethylation, hydroxylation, and dechlorination in vitro. Totaling five reactive metabolites, three cyano adducts and two GSH conjugates were identified. Using the Xenosite web-based predictor, the toxicity of DMB and its metabolites were predicted in silico. Metabolism and bioactivation reactions at the pyrimidine and piperazine rings were once assumed to be responsible for DMB's toxicity and instability.

Supplementary Materials: The following supporting information can be downloaded at the website of this paper posted on Preprints.org.

Funding: This research was funded by the Researchers Supporting Projecting, King Saud University, Riyadh, Saudi Arabia, grant number RSP-2023R353.

Acknowledgments: The authors extend their appreciation to the Researchers Supporting Projecting, King Saud University, Riyadh, Saudi Arabia for funding this work through grant no. RSP-2023R353.

Conflicts of Interest: The authors declare that they have no known competing financial interests or personal relationships that could have appeared to influence the work reported in this paper.

References

1. Natoli, C.; Perrucci, B.; Perrotti, F.; Falchi, L.; Iacobelli, S. Tyrosine Kinase Inhibitors. Curr. Cancer Drug Targets 2010, 10 (5), 462–483.
2. Lemmon, M. A.; Schlessinger, J. Cell Signaling by Receptor Tyrosine Kinases. Cell 2010, 141 (7), 1117–1134.
3. Tanaka, M.; Siemann, D. W. Therapeutic Targeting of the Gas6/Axl Signaling Pathway in Cancer. Int. J. Mol. Sci. 2021, 22 (18), 9953.
4. Sinha, S.; Boysen, J. C.; Chaffee, K. G.; Kabat, B. F.; Slager, S. L.; Parikh, S. A.; Secreto, C. R.; Call, T.; Shanafelt, T. D.; Leis, J. F. Chronic Lymphocytic Leukemia Cells from Ibrutinib Treated Patients Are Sensitive to Axl Receptor Tyrosine Kinase Inhibitor Therapy. Oncotarget 2018, 9 (98), 37173.
5. Sen, T.; Tong, P.; Diao, L.; Li, L.; Fan, Y.; Hoff, J.; Heymach, J. V; Wang, J.; Byers, L. A. Targeting AXL and MTOR Pathway Overcomes Primary and Acquired Resistance to WEE1 Inhibition in Small-Cell Lung CancerAXL/MTOR–Mediated WEE1 Inhibitor Resistance in SCLC. Clin. Cancer Res. 2017, 23 (20), 6239–6253.
6. Aveic, S.; Corallo, D.; Porcù, E.; Pantile, M.; Boso, D.; Zanon, C.; Viola, G.; Sidarovich, V.; Mariotto, E.; Quattrone, A. TP-0903 Inhibits Neuroblastoma Cell Growth and Enhances the Sensitivity to Conventional Chemotherapy. Eur. J. Pharmacol. 2018, 818, 435–448.
7. Li, F.; Lu, J.; Ma, X. Profiling the Reactive Metabolites of Xenobiotics Using Metabolomic Technologies. Chem. Res. Toxicol. 2011, 24 (5), 744–751.
8. Al-Shakliah, N. S.; Attwa, M. W.; Kadi, A. A.; AlRabiah, H. Identification and Characterization of in Silico, in Vivo, in Vitro, and Reactive Metabolites of Infigratinib Using LC-ITMS: Bioactivation Pathway Elucidation and in Silico Toxicity Studies of Its Metabolites. RSC Adv. 2020, 10 (28), 16231–16244.
9. Bolton, J. L.; Trush, M. A.; Penning, T. M.; Dryhurst, G.; Monks, T. J. Role of Quinones in Toxicology. Chem. Res. Toxicol. 2000, 13 (3), 135–160.
10. Ma, S.; Zhu, M. Recent Advances in Applications of Liquid Chromatography–Tandem Mass Spectrometry to the Analysis of Reactive Drug Metabolites. Chem. Biol. Interact. 2009, 179 (1), 25–37.
11. Stepan, A. F.; Walker, D. P.; Bauman, J.; Price, D. A.; Baillie, T. A.; Kalgutkar, A. S.; Aleo, M. D. Structural Alert/Reactive Metabolite Concept as Applied in Medicinal Chemistry to Mitigate the Risk of Idiosyncratic Drug Toxicity: A Perspective Based on the Critical Examination of Trends in the Top 200 Drugs Marketed in the United States. Chem. Res. Toxicol. 2011, 24 (9), 1345–1410.
12. Tolonen, A.; Turpeinen, M.; Pelkonen, O. Liquid Chromatography–Mass Spectrometry in in Vitro Drug Metabolite Screening. Drug Discov. Today 2009, 14 (3–4), 120–133.
13. Attwa, M. W.; Kadi, A. A.; Darwish, H. W.; Amer, S. M.; Al-Shakliah, N. S. Identification and Characterization of in Vivo, in Vitro and Reactive Metabolites of Vandetanib Using LC–ESI–MS/MS. Chem. Cent. J. 2018, 12 (1), 1–16.
14. DiMasi, J. A.; Hansen, R. W.; Grabowski, H. G. The Price of Innovation: New Estimates of Drug Development Costs. J. Health Econ. 2003, 22 (2), 151–185.
15. Raies, A. B.; Bajic, V. B. In Silico Toxicology: Computational Methods for the Prediction of Chemical Toxicity. Wiley Interdiscip. Rev. Comput. Mol. Sci. 2016, 6 (2), 147–172.
16. Matlock, M. K.; Hughes, T. B.; Swamidass, S. J. XenoSite Server: A Web-Available Site of Metabolism Prediction Tool. Bioinformatics 2015, 31 (7), 1136–1137.
17. Zaretzki, J.; Matlock, M.; Swamidass, S. J. XenoSite: Accurately Predicting CYP-Mediated Sites of Metabolism with Neural Networks. J. Chem. Inf. Model. 2013, 53 (12), 3373–3383.
18. Dang, N. Le; Hughes, T. B.; Krishnamurthy, V.; Swamidass, S. J. A Simple Model Predicts UGT-Mediated Metabolism. Bioinformatics 2016, 32 (20), 3183–3189.
19. Jia, L.; Liu, X. The Conduct of Drug Metabolism Studies Considered Good Practice (II): In Vitro Experiments. Curr. Drug Metab. 2007, 8 (8), 822–829.
20. Al-Shakliah, N. S.; Attwa, M. W.; AlRabiah, H.; Kadi, A. A. Identification and Characterization of in Vitro, in Vivo, and Reactive Metabolites of Tandutinib Using Liquid Chromatography Ion Trap Mass Spectrometry. Anal. Methods 2021, 13 (3), 399–410.
21. Al-Shakliah, N.; Kadi, A.; Al-Salahi, R.; Rahman, A. F. M. In Vitro Identification of Potential Metabolites of Plinabulin (NPI 2358) in Hepatic Preparations Using Liquid Chromatography–Ion Trap Mass Spectrometry. ACS Omega 7 (25), 21465–21472. https://doi.org/10.1021/acsomega.2c00929.
22. Jian, W.; Liu, H.-F.; Zhao, W.; Jones, E.; Zhu, M. Simultaneous Screening of Glutathione and Cyanide Adducts Using Precursor Ion and Neutral Loss Scans-Dependent Product Ion Spectral Acquisition and Data Mining Tools. J. Am. Soc. Mass Spectrom. 2012, 23 (5), 964–976.
23. Xie, C.; Zhong, D.; Chen, X. A Fragmentation-Based Method for the Differentiation of Glutathione Conjugates by High-Resolution Mass Spectrometry with Electrospray Ionization. Anal. Chim. Acta 2013, 788, 89–98.

 doi:10.20944/preprints202305.1022.v1

24. Abdelhameed, A. S.; Attwa, M. W.; Kadi, A. A. Characterization of Stable and Reactive Metabolites of the Anticancer Drug, Ensartinib, in Human Liver Microsomes Using LC-MS/MS: An in Silico and Practical Bioactivation Approach. Drug Des. Devel. Ther. 2020, 14, 5259.